Applied Physics A (2026) 132:236
https://doi.org/10.1007/s00339-026-09444-y

**Applied Physics A**
**Materials Science & Processing**

# Characterisation of low crystallinity CNTs incorporated zinc silicate ceramic composites: Morphology, optical, dielectric and microhardness properties

**Kar Fei Chan[1,3] · Md Shuhazlly Mamat[1] · Mohd Hafiz Mohd Zaid[1] · Masaki Tanemura[2] · Mohd Zamri Mohd Yusop[3] · Takahiro Maruyama[4] · Kamal Prasad Sharma[4] · Shahira Liza[5] · Yazid Yaakob[1,6]**

Received: 21 September 2025 / Accepted: 16 February 2026


## Abstract

Carbon nanotubes has been researched deeply as a reinforced material, since it showed good properties in different matrices, yet the aggregation issue has always been brought up to restrain its applicability. Carbon nanotubes' rapid electronic conductivity was expected to enhance the ceramic composite specifically zinc silicate as the potential candidate of the fluorescent materials. In this study, low crystallinity carbon nanotubes (CNTs) synthesized by chemical vapor deposition were mixed with zinc silicate made by melt-quenching to fabricate the CNTs incorporated zinc silicate composites. The composites were analyzed using Raman, XPS, FESEM, UV-Vis, LCR and Vicker's microhardness tester. It was found that the optical bandgap energy of the CNTs added composites a decay in the optical bandgap while the luminescence behavior remains unchanged. The FESEM image revealed that the composite included CNTs pullout and aggregation. LCR analysis showed that ZS/CNT-x composites have a higher AC conductivity value, together retain their non-ohmic conductivity with the unchanged molecular structure. Through this study, the results allowed the CNTs ceramic research path to be served the scientific community in the development of narrow bandgap material with the wide bandgap compound as the starting material.

**Keywords** Carbon nanotubes · Zinc silicate · Optical bandgap · Dielectric constant

## 1 Introduction

Since its pioneer publication in 1991 [1], nano carbons such as carbon nanotubes have been recognised as the wonder material and extensively studied in numerous research fields. Chemical vapor deposition (CVD), one of the established production methods, needed relatively low operating costs. As the carbon atom's growth site during the CVD process, a metal catalyst with moderate carbon solubility was required. The desired crystallinity of the nanotubes can be manipulated by adjusting the reaction temperature, heating time, and cooling time [2]. Low crystallinity nanocarbon can be achieved by keeping the reaction temperature below 1000 °C and shortening the reaction time [3]. Previously, researchers were performed experimentally to identify the effectiveness of low crystallinity carbon nanotubes in different domain or application, compared to the high crystallinity nanotubes. Rathore et al. reported the effectiveness of nanotubes to the optical bandgap energy of the poly(3-hexylthiophene)

✉ Yazid Yaakob
yazidakob@upm.edu.my

1 Department of Physics, Faculty of Science, Universiti Putra Malaysia, Serdang 43400, Selangor, Malaysia

2 Department of Physical Science and Engineering, Graduate School of Engineering, Nagoya Institute of Technology, Gokiso-cho, 466-8555, Showa-ku, Nagoya, Japan

3 Department of Materials, Manufacturing and Industrial Engineering, Faculty of Mechanical Engineering, Universiti Teknologi Malaysia, Skudai 81310, Johor, Malaysia

4 Nanomaterial Research Centre, Meijo University, Tempaku-ku, Nagoya 468-8502, Japan

5 TriPrem I-Kohza, Malaysia-Japan International Institute of Technology, Universiti Teknologi Malaysia, Kuala Lumpur 54100, Malaysia

6 Halal Products Research Institute, Universiti Putra Malaysia, Serdang 43400 UPM, Selangor, Malaysia

Published online: 02 March 2026

composite for its potential application as polymer-based optoelectronic device [4]. They discovered the photon absorption peak of the composite shift to longer wavelength, and the composites experienced a decline in optical bandgap energy due to the increase in conjugation length between the polymer chains and nanotubes.

Besides, Da Luz et al. discussed about the applicability of pristine nanotubes and treated nanotubes in the metakaolin-based geopolymer, claiming that the yield stress of the geopolymer did not beneficial from the nanotubes [5]. Yet, the acid-treated nanotubes reduce the amount of macropore and improve the microcrack bridging effects. Li et al. also compared the pristine and functionalized carbon nanotubes with respected $I_D/I_G$ ratio at 0.83 and 0.85, as the mechanical and biocompatibility enhancement in the hydroxyapatite composites [6]. It was found that the added nanotubes with higher $I_D/I_G$ ratio showed higher flexural strength and higher osteoblast cells viability, ascribing to the more effective mechanical load transfer and greater cells adhesion on the composites.

Currently, mass quantities of optoelectronic devices have been manufactured to permeate modern society's communications, computer, entertainment, and lighting sectors. Optoelectronic materials refer to the core materials that contribute to the development of optoelectronic devices. Numerous studies on the optoelectronic properties of ceramics based on zinc silicate have been conducted, including band gap research, luminescence research, and photon-electron interaction [7, 8]. However, it was challenging to increase electrical conductivity of this ceramic without compromising its optimum luminosity. Abdel Wahab et al. lowered the optical bandgap energy of zinc silicate glass composite through the addition of high melting point element – tungsten ion ($W^{6+}$) [9]. From the direct bandgap calculation, the added $W^{6+}$ ion successfully lowered the bandgap energy of the composite from 2.82 to 2.41 eV, attributed to the variation of charge on the W atom causing the imperfection states between the conduction band and the valence band. In addition, the mesoporous zinc silicate composites reached a high surface hardness and antibacterial properties for dental resin composites [10]. Before the doping process, the hardness of the mesoporous composite was recorded at 26.89 HV, and it only increased to 36.2 HV when 5% zinc oxide was doped to the composites.

Low-crystallinity or highly amorphous CNTs, often considered a disadvantage in laboratory- and industrial-scale applications, have rarely been explored for this purpose. In this study, the effects of low-crystallinity CNTs on the performance of ZS composites are systematically investigated, with particular emphasis on their influence on electrical conductivity and optical properties. The use of low-crystallinity CNTs, characterized by random orientation and amorphous regions, was proposed as a novel approach to form a conductive carbon network within the ZS matrix. This work aims to provide a deeper understanding of the interactions between CNTs and ZS ceramics and to elucidate their contribution to the overall optical and electrical performance enhancement, offering new insights into the potential application of amorphous CNTs in ceramic composite materials.

## 2 Methodology

### 2.1 Sample preparation

#### 2.1.1 Carbon nanotubes

Refer to the earlier report [11] for information regarding the synthesis of carbon nanotubes and CNT-zinc silicate composites. The nanotubes were synthesized from cobalt (II, III) oxide nanopowder ($Co_3O_4$, < 50 nm particle size, 99.5% trace metal basis, Sigma-Aldrich) as metal catalyst and Ethanol ($C_2H_5OH$, 95% technical grade, SYSTERM) as carbon precursor through chemical vapour deposition. $Co_3O_4$ powder was weighed and sintered up to 800 °C with ramping rate 10°C$min^{-1}$ in an argon environment. At 800 °C, the mixture of vaporised ethanol, argon gas (Ar, 50 sccm) and hydrogen gas ($H_2$, 5 sccm) was introduced into the furnace for 30 min deposition time. The sample was then annealed to ambient temperature in the Ar environment, and the sample was labelled as CNTs.

#### 2.1.2 Carbon nanotubes incorporated zinc silicate (ZS) composite

The CNTs were mixed using pestle and mortar at the CNTs mass fractions of 0.2, 0.4, 0.6, 0.8, 1.0, 2.0 and 3.0 w.t.% relative to the mass of ZS. The powder mixture was pelletized at the 5 tonnes for 10 min with the binding agent (0.5 ml polyvinyl alcohol (PVA) per 1 g mixture). After pelleting, the pellets were sintered at 800 °C for two hours and then annealed to ambient temperature in an Ar environment. The Ar flow rate, ramp temperature and annealing duration were 50 sccm, 10°C$min^{-1}$ and 6 h, respectively. The CNTs incorporated zinc silicate ceramic composites were abbreviated as ZS/CNT-x, where x was the CNTs mass fractions.

### 2.2 Characterisation

The surface chemistry of the composites was characterized via a Raman Scattering Spectrometer (NRS-3300, JASCO, Japan) and X-ray Photoelectron Spectrometer (XPS, JPS-9200, JEOL, Japan). The Raman spectra were collected with a diode-pumped solid-state laser with wavelengths of

532.06 nm, while the XPS analysis was performed with a monochromatic MgKα X-ray source (1253 eV). The surface topography of the composites was observed through an optical microscope (VHX-500, Keyence, Japan) at the magnification of 500×, and the electron micrographs (magnification: 500× and 25,000×) was collected using a scanning electron microscope (SEM, JSM-5600, JEOL, Japan) at the 5.0 kV accelerating voltage.

The photon absorption of the composites was analysed with ultraviolet-visible light spectrophotometer (UV-Vis, UV-3600, Shimadzu, Japan) at the illuminated wavelength from 220 to 700 nm. The optical bandgap ($E_{opt}$) was estimated by a linear fitting at the slope in the UV-Vis spectra and extrapolating to the zero absorption at the function of the wavelength. The luminescence properties of the composites were investigated using a photoluminescence spectrometer (PL, LS55, Perkin Elmer, United States of America) at the excitation wavelength of 260 nm. To determine the perceived colour in human colour vision, the emission spectra was inputted into the International Commission on Illumination (CIE) 1931 chromaticity diagram. From the CIE 1931, the distribution of wavelengths in visible spectrum was defined quantitatively into x- and y-coordinate.

Next, the dielectric properties of composites were measured with impedance-capacitance-resistance bridge (LCR, HM8118, Rohde & Schwarz, Germany) at the frequency ranging from 20 Hz to 200 kHz for the AC conductivity and dielectric constant. The bulk density of ZS/CNT-x composites was determined using densimeter (MD-300 S, Alfa-Mirage, Japan) with distilled water as the measuring medium, while the Vickers microhardness tester (HMV-G21S, Shimadzu, Japan) measured the surface hardness through a 30 s indentation with force $H_V0.1$ (980.7 mN).

## 3 Results and discussions

### 3.1 Surface chemistry and topography of composites

Figure 1(a) shows the defect (D) and graphitization (G) bands coexisted in the sample CNTs and ZS/CNT-1.0. In the Raman spectrum of CNTs, it indicated that the as-synthesised CNTs containing the cobalt element with $A_{1g}$ mode where the respective wavenumber located at 700 $cm^{-1}$. As shown in our previous work [11] and Figure S1 and S2, the XRD spectrum and micrographs of synthesized CNTs showed the amorphous carbon had successfully coated the Co nanoparticles. In contrast, the spectrum of ZS/CNT-1.0 sample showed the corresponding functional group which are the Zn, Si, and Si-O-Si, making the zinc silicate composite a polymeric structure. Moreover, through the Raman scattering-based Cançado model [12], the measured $I_D/I_G$ ratio was used to calculate the crystallite size of the nanocarbon content which refer to the CNTs within the composite. The crystallite size of as-synthesized CNTs was 17.03 nm ($I_D/I_G$ = 1.13), whereas it was 19.36 nm ($I_D/I_G$ = 0.99) for ZS/CNT-1.0 composite. During the fabrication of ceramic composites, the carbon structure underwent additional crystallization at a higher temperature at 800°C. The peak at 2684 $cm^{-1}$ represented the G' band (second order Raman overtone).

In addition, XPS revealed the surface chemical characteristics of the ZS/CNT-1.0 sample. The broad scan spectra in Fig. 1(b) revealed that the composites contained the elements Si, Zn, O, and C, with photoelectron lines positioned at 99 eV (Si 2p), 91 eV (Zn $3p_{1/2}$), 528 eV (O 1 s), and 284 eV (C 1 s). Figure 1(c) showed the high-resolution Si 2p scan which indicated the chemical bonding existed in the Si 2p: Si, Si-C, Si-O-Si and Si-O. In Fig. 1(d), the C 1 s high-resolution scan revealed the presence of graphitic carbon (284.6 eV), carboxyl (288.1 eV), and satellite peak due to an abrupt change in the Columbic potential (276.1 eV). Table 1 also depicted the corresponding binding energy position for certain chemical bonding between sample ZS/CNT-1.0 and previous reported ZS without CNTs addition. With the standardized C 1 s charge correction, the binding energy of the ZS/CNT-1.0 sample shifted to the left, as compared to the ZS sample in the previous report [13]. This indicates that the radical carbon invasion altered the domain molecules slightly and achieved a higher oxidation state [14].

Figure 2 depicted digital micrograph and FESEM micrographs of the ZS/CNT-1.0 sample. Figure 2(a) showed three dispersion behaviour on the composite surface which are the regions without CNTs, the regions with dispersed CNTs and the regions with aggregated CNTs. The as-synthesised CNTs with low crystallinity and expected lower chemical inertness enables a higher degree of chemical interaction between CNTs and the zinc silicate domain, leading to the dispersed CNTs behaviour within the composite. However, the computed crystallite size of CNTs is relatively lower compared to the commercial CNTs, the aggregation still occurred within the composite revealing the inevitable aggregation nature of the low dimension material. Figure 2(b) and (c) revealed that two CNTs behaviours- aggregation and pullout, coexisted in the composite. CNTs aggregated inevitably due to the minimum interfacial bonding with the domain ceramic. Nonetheless, a tiny amount of CNTs pullout was seen, which was attributed to defect sites and an amorphous phase. At elevated temperatures, the amorphous carbon phase was more reactive with zinc silicate (the domain crystal system), than crystallite carbon structure.

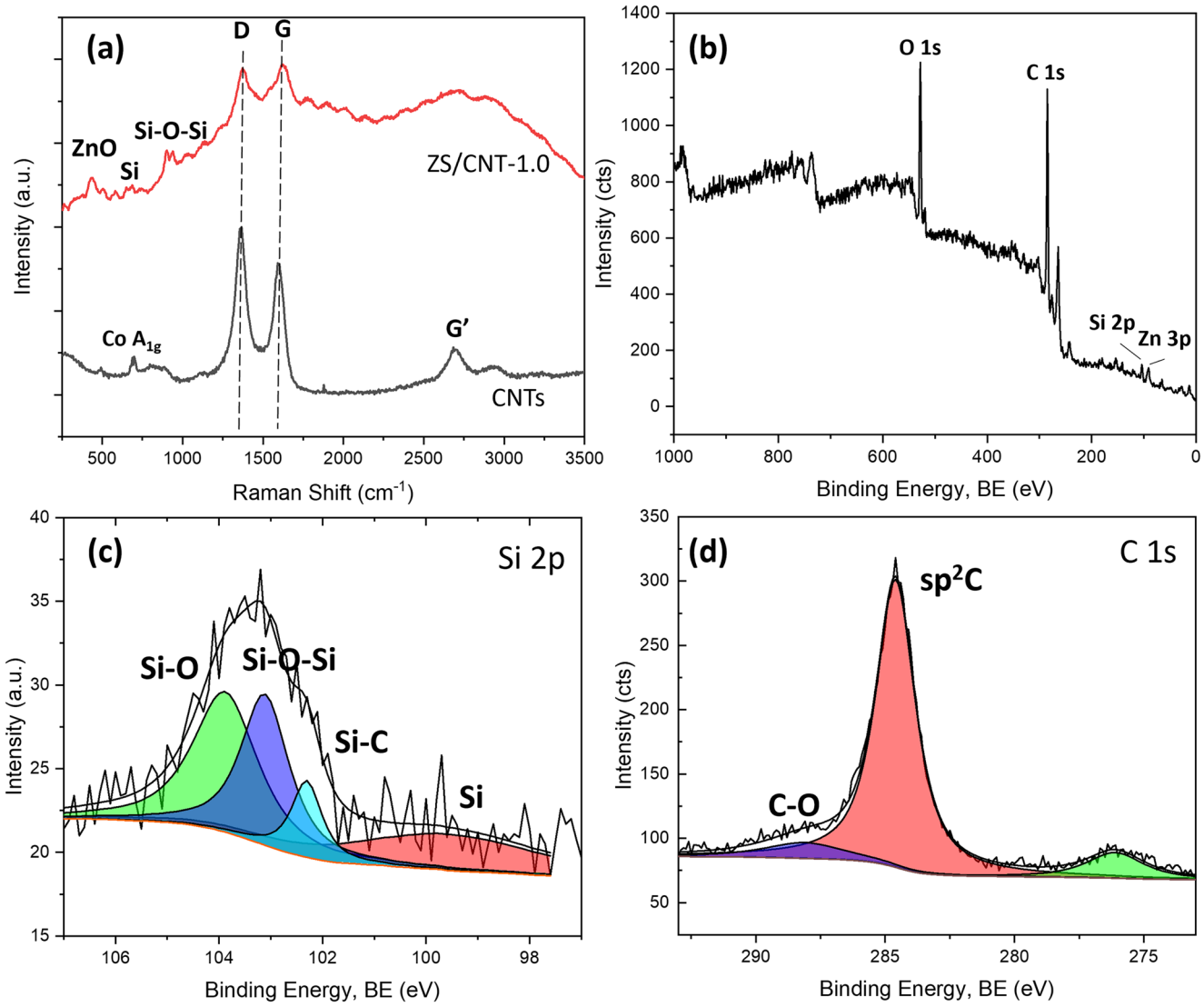


**Fig. 1** The surface chemistry analysis: (**a**) Raman Spectra of added CNT and CoCNT-1.0 composite, (**b**) XPS wide scan spectrum of CoCNT-1.0 composite, (**c**) Si 2p narrow scan spectrum, and (**d**) C 1 s narrow scan spectrum

**Table 1** Binding energy respected to the chemical bonding, obtained from deconvoluted high resolution Si 2p and C 1 s spectra

| Sample | Binding Energy, BE (eV) | | | | References |
|---|---|---|---|---|---|
| | Si-O-Si | Si-O | $sp^2C$ | C-O | |
| ZS | 102.6 | 103.4 | 284.4 | 289.4 | [13] |
| ZS/CNT-1.0 | 103.1 | 103.9 | 284.6 | 288.1 | This work |

### 3.2 Photon absorption and luminescence

Figure 3(a) showed the photon absorption of the composites across the UV and visible light region, showing that the light absorbance increased with the CNTs addition. Regardless of the CNTs addition, the spectra showed an identical UV absorption peak ranged from 321 to 347 nm, which categorized as the Zinc absorption peak. Figure 3(b) displayed the optical bandgap energy ($E_{opt}$) derived from the UV-Vis and Tauc plots (the interpretation technique can be found in the previous report [15]). The value of $E_{opt}$ decreased as the CNTs' mass increased. $E_{opt}$ denoted the energy required for an electron to "jump" from the valence band to the conduction band, including recombining the electron-hole pair. In this investigation, the direct $E_{opt}$ of zinc silicate was measured to be 3.07 eV, and the values of ZS/CNT-x composites were fitted with a first-order exponential decay, as depicted in Fig. 3(b). Since the composite retained its heterogeneous structure, as evidenced by the micrographs in Fig. 3 of the aggregated CNTs, the

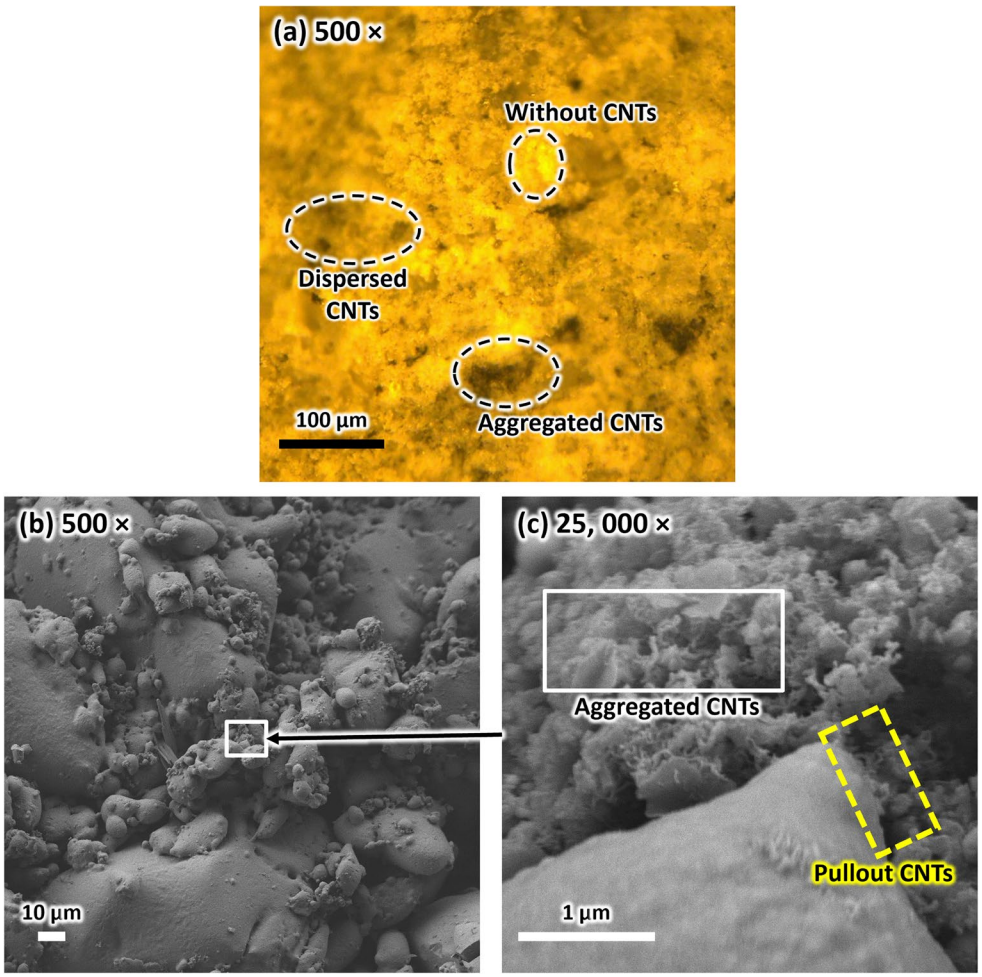


**Fig. 2** Surface topography observation of ZS/CNT-1.0 composite: (**a**) Optical microscope, (**b**) and (**c**) FESEM micrographs at different magnification

decline in $E_{opt}$ may have been caused by the high photon absorption of the CNTs rather than the modification of zinc silicate's band structure [16]. The electron trap introduced by the CNTs was another reason that contributed to the decline in $E_{opt}$. During photoexcitation, the graphitic structure disintegrated into $E_{22}$ electrons to generate electron traps, which tend to reduce the $E_{opt}$ of the zinc silicate ceramic domain.

As a comparison with our work [15], the $E_{opt}$ of the ZS/CNT-x in this study showed different decay differ to the linear decay in the previous report. This is expected to the dispersion homogeneity of carbon content in the composite, where the incident ray from the UV-Vis analyser was likely to be absorbed and scattered more at the region with the CNTs content with high chemical inertness and highly aggregated in an inhomogeneous ZS/CNT composite. Hence, the expected lower chemical inertness of the as-synthesised CNTs showed higher distribution homogeneity, and the $E_{opt}$ of the composites decreased in an exponential decay order.

The luminescence behaviour of the composites under the UV excitation was shown in Fig. 3(c) – (d). As reported in the previous literature, the zinc silicate composite with nanocarbon addition emitted near-ultraviolet (NUV, 366.5 nm), yellowish-green visible light (572 nm), and near-infrared radiation (NIR, 756 nm). The emission peak located at 780 nm in the spectra was related to the second diffraction of the PL analyser's excitation ray, which was neglected in the discussion. Throughout the CNTs addition, the emission peaks of the composite did not alter significantly by the Co content nor the C content. The emission peak in the PL spectra changed when there are additional metal ions been introduced into the domain matrix, such as an addition of transition metal and rare earth ions with different energy levels [17, 18]. In addition, the computed x- and y- coordinates, shown in Fig. 3(d) and Table 2, provided an additional information to the PL spectra where the emitted colour only undergo a minor change to the typical human vision. From the literature study [19], the cobalt oxide-added zinc silicate composite emitted red (602 nm) and infrared (717 nm) under the excitation at 400 nm. The emission peaks are due to the d-d vibronic transition of $^4A_2(F) \rightarrow {}^4T_1(^4P)$ transition [20]. However, in a low-oxygen sintering environment, the graphitic structure experienced minimum thermal oxidation

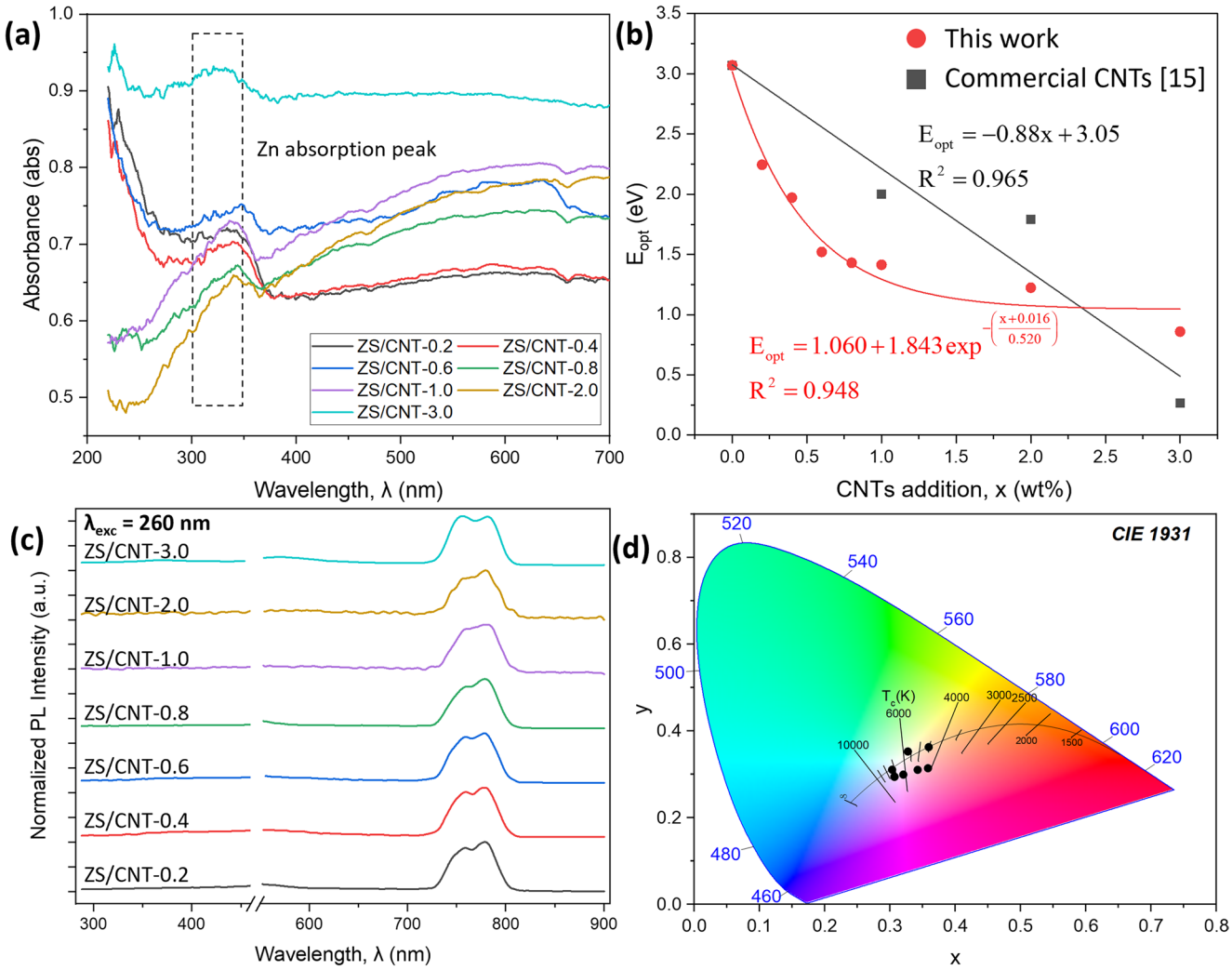


**Fig. 3** Optical absorption and emission spectra of the composites: (**a**) UV-Vis absorption spectrum, (**b**) optical bandgap spectrum, (**c**) PL spectrum and (**d**) computed CIE 1931

**Table 2** The estimated optical bandgap energy $E_{opt}$, electron transition, CIE 1931 coordinates of the fabricated composites

| Sample | $E_{opt}$ (eV) | Electron Transition | X-coordinate in CIE 1931 | Y-coordinate in CIE 1931 |
|---|---|---|---|---|
| ZS | 3.07 [15] | Direct Forbidden | 0.355 | 0.340 |
| ZS/CNT-0.2 | 2.25 | | 0.304 | 0.309 |
| ZS/CNT-0.4 | 1.97 | | 0.307 | 0.294 |
| ZS/CNT-0.6 | 1.52 | | 0.321 | 0.298 |
| ZS/CNT-0.8 | 1.43 | | 0.328 | 0.353 |
| ZS/CNT-1.0 | 1.41 | | 0.344 | 0.316 |
| ZS/CNT-2.0 | 1.22 | | 0.369 | 0.328 |
| ZS/CNT-3.0 | 0.86 | | 0.357 | 0.353 |

or degradation. The graphitic structure was expected to encapsulate the catalyst and limits the diffusion of $Co^{2+}$ ions into the zinc silicate lattice. The carbon encapsulation enables the change in electron transport and limits the metal ions transfer into the ceramic matrix, leading to a minute change to the luminescence behaviour of the composite.

### 3.3 AC conductivity and dielectric constant

Figure 4(a) depicted the value of AC conductivity as a function of frequency. The graph demonstrated that the conductivity increased with increasing frequency, indicating that the sample composites behaved as non-ohmic conductors

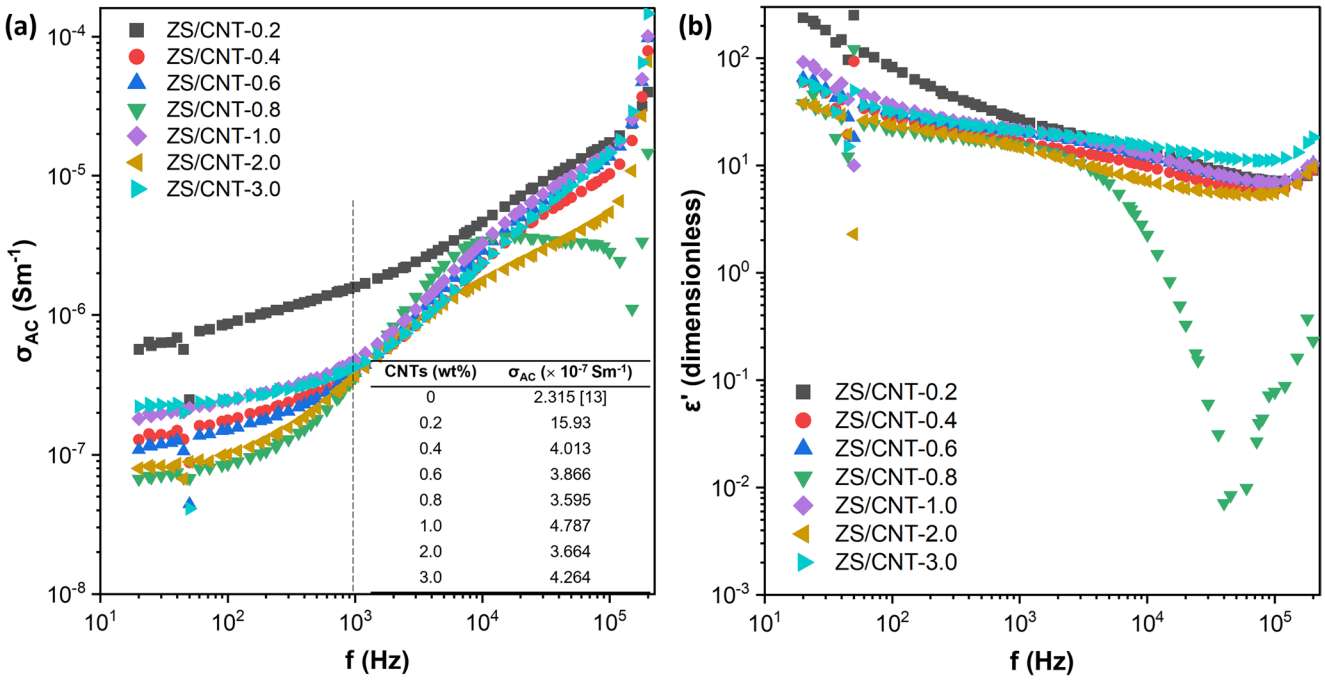


**Fig. 4** Variation of dielectric properties of the composites with frequency: (**a**) AC conductivity, (**b**) Dielectric constant of composites with min. thermal oxidation and (**c**) dielectric constant of composites with moderate thermal oxidation

regardless of the presence of CNTs. As previously reported, the AC conductivity of zinc silicate ceramic composite is $2.315 \times 10^{-7}$ $Sm^{-1}$ at 1000 Hz [13]. Based on Fig. 4(a), the ZS/CNT composites shared the same trend as the ZS sample, which the conductivity increased with the measuring frequency. This paper provided evidence indicating that the CNTs addition did not alter the band structure of the ceramic structure which is non-ohmic behaviour. As the CNTs did not modify the band structure, the AC conductivity of ZS/CNT composites did not improve significantly at either low or high CNT loadings, where the low crystallinity of the CNTs played a critical role [21–23]. The formation of an effective electrically conductive pathway requires a continuous carbon network with CNTs oriented parallel to the current flow. However, the excessive incorporation of low-crystallinity CNTs in the ZS ceramic composite led to random orientation and amorphous regions, which can trap charge carriers and significantly hinder the formation of efficient conductive pathways.

The variation of dielectric constant (ε') of the composite with the measuring frequency was shown in Fig. 4(b). Figure 4(b) showed the dielectric constant of the composites with minimum thermal oxidation. Despite the oxidation, both composites experienced the decline of dielectric constant across the frequency due to the Maxwell-Wagner-Sillars polarisation for heterogeneous system [24]. The external electromagnetic (EM) field changed rapidly with the increased applied frequency. The random dipoles within the composites unable to complete the rearrangement of the orientations parallel to the external EM field, leading to the polarisation of the dielectric properties [25]. In fact, the improved ε' with the CNTs addition was assigned to the enhanced interfacial polarisation through the interface coupling between CNTs and ceramic domain. The result was in agreement with the work done by Wu et al. about the improvement of ε' in ZS/CNT composites was ascribed to the formation of microcapacitors by CNTs [26].

### 3.4 Surface Microhardness and Bulk Density

Figure 5 showed the Vickers' microhardness (HV) and bulk density of the CNTs-added composite, along with the relative porosity. Before the CNTs addition, the reported bulk density and microhardness of the zinc silicate composite was 3.56 $gcm^{-3}$ and 285 HV [13]. The Vickers hardness of the ZS/CNTs composites decreased with increasing CNT content. A notable difference between commercial and synthesized CNTs is the fluctuation in hardness measurements: composites with commercial CNTs exhibit smaller deviations, while those with synthesized CNTs show larger fluctuations. This behaviour can be attributed to the presence of Co nanoparticles within the synthesized CNTs. The carbon-coated Co does not react with the ZS matrix during sintering, remaining as discrete particles randomly distributed near the composite surface, which affects the distribution of applied load during hardness testing. Correspondingly,

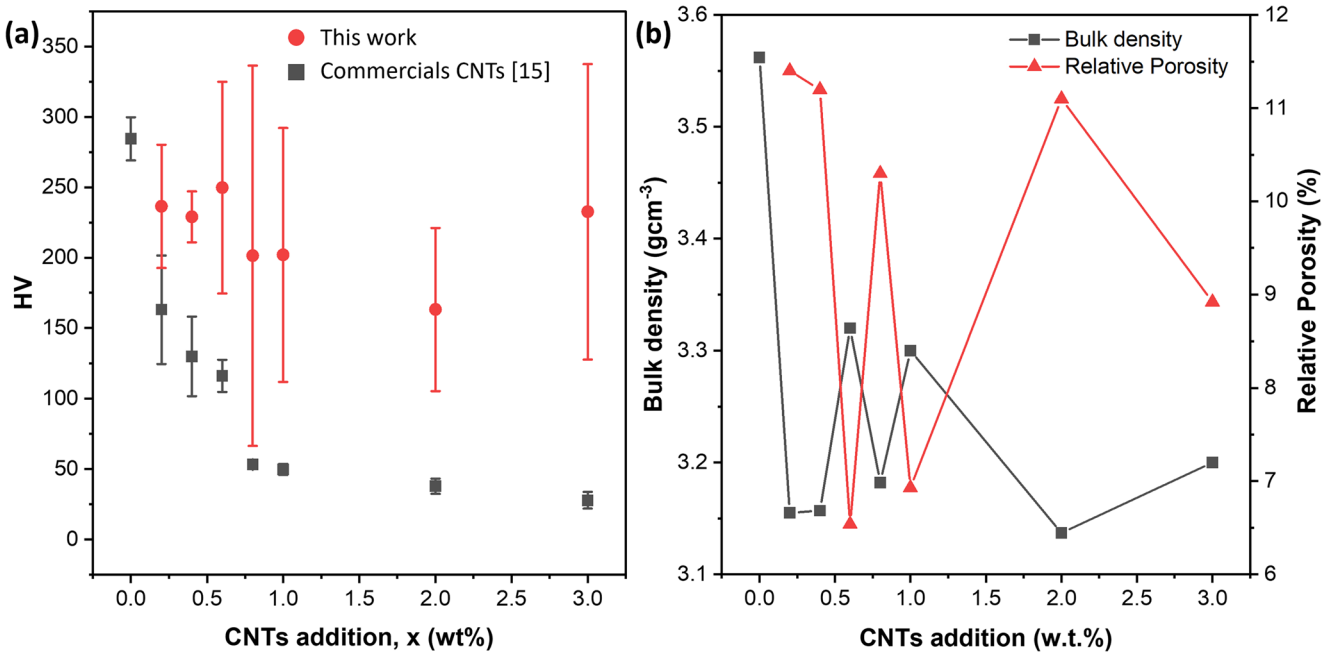


**Fig. 5** Variation of bulk density and Vicker's microhardness with the function of CNT addition

the bulk density of the composites also decreased with CNT addition, reflecting an increase in porosity. The high porosity (up to 11.4%) was attributed to the high aggregation rate of high-loading CNTs would make it difficult to enter the fractured or vacant sites of the ceramic. Notably, the intertube distance between CNTs reduced when the CNTs loading is high. With the hydrophobic and low solubility behaviour, the CNTs tend to aggregate and form cluster. The CNTs cluster with low intertube distance influenced negatively to the Nusselt and Reynold number, which determines the effectiveness of energy transfer [27]. Despite these fluctuations, the overall trends in hardness and density remain consistent, supporting the conclusion that CNTs incorporation influences the mechanical properties of the ZS composites.

Subjected to the bulk density and microhardness, compared to the previous report using the commercial CNTs via powder processing [13], the decreasing trend of the composite series was relatively slower. This also attributed to the mixed state (amorphous – crystalline) phases and low aspect ratio of the synthesised CNTs [28]. Low crystallinity CNTs with low aspect ratio extend like the deformed chain link under high shear rate. These factors reduced the risk of CNTs aggregation and create pores within the ceramic composites. However, the crystallite size of CNTs increased after the densification and sintering process, leading to the increase in chemical inertness. The increased chemical inertness reduced the interfacial adhesion between CNTs and zinc silicate ceramic, leading to the decay in surface hardness.

## 4 Conclusions

To sum up, multiple properties were characterized on the synthesised CNTs incorporated zinc silicate ceramic composites which were fabricated through powder processing. Raman scattering showed that the crystallite size of CNTs increased after the composite-mixing process, reducing the interfacial adhesion in the composites. The declining surface hardness was a result of the low chemical interaction. In addition, the composites' optical bandgap energy ($E_{opt}$) showed a first-order exponential decay as a function of CNTs weightage. Referring to the XPS spectrum, the added CNTs does not modify the binding energy of the domain ceramic significantly. Hence, it can be deduced that the composites retained their non-ohmic electronic band structure. The as-synthesised CNTs, with low crystallite size and expected low chemical inertness, achieved a higher dispersion order, and showed an exponential decay of the $E_{opt}$ value. The Co inclusion in the composite was expected to modify the electronic structure and the matrix arrangement, yet the inclusion did not alter the structure nor the matrix. The Co was encapsulated with the layered carbon, making it inert to the surrounding and showed minimum enhancement factors to the composites. The presented results can be referred to as a consideration during the experimental design of nanotube/ceramic composites in the phosphor devices development.

**Supplementary Information** The online version contains supplementary material available at https://doi.org/10.1007/s00339-026-09444-y.

**Acknowledgements** This study was supported by Universiti Putra Malaysia through Geran Putra-Inisiatif Putra Siswazah (GP-IPS/2022/9724300), Insentif Geran Putra (GPI/2023/9763300) and Nanotechnology Platform Program < Molecule and Material Synthesis > of the Ministry of Education, Culture, Sports, Science and Technology (MEXT), Japan.

**Author contributions** Kar Fei Chan: Writing – Original Draft, Investigation, Methodology; Md Shuhazlly Mamat: Writing - Review & Editing, Supervision; Mohd Hafiz Mohd Zaid: Resources, Supervision Masaki Tanemura: Funding acquisition; Mohd Zamri Mohd Yusop: Validation; Takahiro Maruyama: Resources Kamal Prasad Sharma: Resources; Shahira Liza: Validation; Yazid Yaakob: Project administration, Funding acquisition, Supervision, Conceptualisation.

**Funding** Open access funding provided by The Ministry of Higher Education Malaysia and Universiti Putra Malaysia.

## Declarations

**Competing Interests** The authors declare that they have no conlicts of interest to disclose. They conirm that there are no competing interests related to this study.



## References

1. S. Iijima, Nature. **354**, 56 (1991)
2. L. Ci, B. Wei, C. Xu, J. Liang, D. Wu, S. Xie, W. Zhou, Y. Li, Z. Liu, D. Tang, J. Cryst. Growth **233**, 823 (2001)
3. M. Robaiah, M. Rusop, S. Abdullah, Z. Khusaimi, H. Azhan, M.Y. Fadzlinatul, M.J. Salifairus, N.A. Asli, in *AIP Conf. Proc.* (2018), p. 020027
4. P. Rathore, C.M.S. Negi, A.S. Verma, A. Singh, G. Chauhan, A.R. Inigo, S.K. Gupta, Mater. Res. Express. **4**, 085905 (2017)
5. G. da Luz, P.J.P. Gleize, E.R. Batiston, F. Pelisser, Cem. Concr. Compos. **104**, 103332 (2019)
6. H. Li, X. Song, B. Li, J. Kang, C. Liang, H. Wang, Z. Yu, Z. Qiao, Mater. Sci. Eng. C, Mater. Biol. Appl. **77**, 1078 (2017)
7. M. Bala, S. Pawaria, N. Deopa, S. Dahiya, A. Ohlan, R. Punia, A.S. Maan, J. Mol. Struct. **1234**, 130160 (2021)
8. R. Oueslati-Omrani, A.H. Hamzaoui, Mater. Chem. Phys. **242**, 122461 (2020)
9. E.A.A. Wahab, K.S. Shaaban, A.M. Al-Baradi, Silicon. **14**, 4915 (2022)
10. X. Bai, C. Lin, Y. Wang, J. Ma, X. Wang, X. Yao, B. Tang, Dent. Mater. **36**, 794 (2020)
11. K.F. Chan, M.H. Mohd Zaid, S. Liza, K.A. Matori, M.S. Mamat, M.A. Hazan, Y. Yaakob, Mater. Res. Express. **7**, 105601 (2020)
12. L.G. Cançado, K. Takai, T. Enoki, M. Endo, Y.A. Kim, H. Mizusaki, A. Jorio, L.N. Coelho, R. Magalhães-Paniago, M.A. Pimenta, Appl. Phys. Lett. **88**, 163106 (2006)
13. K.F. Chan, M.H.M. Zaid, M.S. Mamat, M. Tanemura, S. Liza, H. Miyazaki, T. Maruyama, K. Sako, K.P. Sharma, N.H. Osman, Mazlan, Y. Yaakob, Diam. Relat. Mater. **134**, 109772 (2023)., N. K. Sa'at, H. I
14. S.Y. Yang, L. Liu, Z.X. Jia, W.W. Fu, D.M. Jia, Y.F. Luo, Express Polym. Lett. **8**, 425 (2014)
15. K.F. Chan, M.H.M. Zaid, S. Liza, M.S. Mamat, K.A. Matori, N.A. Endot, M. Tanemura, Y. Yaakob, Ceram. Int. **47**, 20108 (2021)
16. S. Iftikhar, M.F. Warsi, S. Haider, S. Musaddiq, I. Shakir, M. Shahid, Ceram. Int. **45**, 21150 (2019)
17. W.M. Cheong, Z.W. Loh, M.H.M. Zaid, J. Mol. Struct. **1248**, 131474 (2022)
18. R.A.A. Wahab, M.H.M. Zaid, K.A. Matori, H.M. Kamari, N.A.M. Yamin, S.N.F. Zalamin, N.A.N. Ismail, S. Honda, M. Tanemura, Macromol. Symp. (2022). https://doi.org/10.1002/masy.202100316
19. S.A.A. Wahab, K.A. Matori, S.H.A. Aziz, M.H.M. Zaid, M.M.A. Kechik, A.Z.K. Azman, R.E.M. Khaidir, M.Z.A. Khiri, N. Effendy, Optik **179**, 919 (2019)
20. K. Tanaka, T. Mukai, T. Ishihara, K. Hirao, N. Soga, S. Sogo, M. Ashida, R. Kato, J. Am. Ceram. Soc. **76**, 2839 (1993)
21. A. Tamayo, J. Mater. Sci. **59**, 877 (2024). M. [a]. A. RodriguezJ. Rubio, and F. Rubio
22. M. Zhu, J. Chen, F. Li, C. Huang, H. Liu, X. Liu, Z. Huang, J. Eur. Ceram. Soc. **43**, 4627 (2023)
23. Y. Oh, M. Heo, Y.W. Kim, H.S. Kim, J. Am. Ceram. Soc. **108**, 1 (2025)
24. R. Megha, Y.T. Ravikiran, S.C. Vijaya Kumari, H.G. Raj Prakash, S.K. Tiwari, S. Thomas, Diamond Relat. Mater. **87**, 163 (2018)
25. Z. Huang, J. Cheng, H. Zhang, Y. Xiong, Z. Zhou, Q. Zheng, G. Zheng, D. Zhang, M. Cao, J. Mater. Sci. Technol. **107**, 155 (2022)
26. W. Wu, T. Liu, D. Zhang, Q. Sun, K. Cao, J. Zha, Y. Lu, B. Wang, X. Cao, Y. Feng, V.A.L. Roy, R.K.Y. Li, Compos. Part A Appl. Sci. Manuf. **127**, 105650 (2019)
27. W. Jeon, J. Ahn, T. Kim, S.M. Kim, S. Baik, ACS Appl. Mater. Interfaces. **12**, 50355 (2020)
28. D.H. Xu, Z.G. Wang, J.F. Douglas, Macromolecules. **41**, 815 (2008)